ELSEVIER

Journal of Nuclear Materials 299 (2001) 101–110

journal of nuclear materials

www.elsevier.com/locate/jnucmat

3D Micromechanical modeling of packed beds

Zi Lu, Mohamed Abdou *, Alice Ying

Mechanical and Aerospace Engineering Department, University of California–Los Angeles, 44-114 Engineering IV, P.O. Box 951597, Los Angeles, CA 90095-1597, USA

Received 5 March 2001; accepted 17 August 2001

Abstract

A new 3D numerical model has been developed to simulate the thermal and mechanical characteristics of packed beds used in fusion reactor blankets and other applications. This method is based on an explicit numerical scheme which monitors the interaction of the particles contact by contact and their motion particle by particle. In this paper, a mathematical formulation as well as a model which predicts the packed bed thermomechanical states under imposed and induced loads are presented. The model is validated by comparing the numerical simulations with thermal expansion and uniaxial compression experiments of packed beds. The results of the calculated bed effective modulus compares reasonably well with the experimental data.

1. Introduction

Packed beds have been considered for shielding and tritium breeding as well as neutron multiplication in fusion reactor blanket designs. During the reactor operation, the blanket structure restrains the expansion of the packed beds and, therefore, causes stresses. The larger expansion of the packed beds in comparison with the surrounding structure is due to a higher coefficient of thermal expansion, higher temperature in the beds and radiation-induced swelling. These stresses may jeopardize the safe blanket operation if the mechanical integrity of the blanket element is endangered or if heat and tritium removals are significantly deteriorated due to particle breakage or melting. The determination of the stresses caused by the packed beds is important in the design of the solid breeder blanket, which requires that the mechanical properties of packed beds be known.

In a particulate medium such as packed beds, forces and heat flows are typically transferred through the contacts between particles. This discrete behavior is very difficult to describe in detail based only on macroscopic experiments or numerical methods like finite element analysis, in which packed beds are modeled as a continuum medium. Whereas the discrete numerical simulations [1–4], in which each particle is treated independently and therefore the discrete nature of particulate medium is preserved, are more flexible in their application and have been successfully applied to analyses of granular materials. Those discrete numerical methods can better quantify the characteristics of particulate materials and remedy the deficiency of the loss of certain information when continuum medium methods are used for discrete particulate materials.

In this paper, a new 3D numerical model is presented to simulate the thermal and mechanical properties of packed beds for fusion reactor blankets. It is a quasi-static model and no transient effects are considered. This model uses the micro-mechanics displacement method in conjunction with an iterative process for the successive releasing of force exerted on each particle. Such a model could provide microscopic insights into thermal–mechanical interactions between particles, and particles with the structural wall, as well as particle relocations at different stages of the reactor operation. Evolution of the particle–particle contact characteristics under internal loading (simulating thermal expansion and radiation swelling), as well as external loading, can be monitored. Simulations are performed to understand the particle bed stress–strain relationship and thermal expansion forces in response

* Corresponding author. Tel.: +1-310 206 0501; fax: +1-310 825 2599.

E-mail address: abdou@fusion.ucla.edu (M. Abdou).

0022-3115/01/$ - see front matter
PII: S0022-3115(01)00690-0

to various loads and conditions. The simulation results are compared with experimental data.

2. Micro-mechanics model

2.1. Normal contact force between two particles

The normal contact force law will be presented for the case of two spheres in contact, sphere 1 and sphere 2 as shown in Fig. 1. The usual tensor notation in the Cartesian coordinate system is adopted. The coordination of the sphere centers are represented as $\mathbf{x}_1$ (x_1, y_1, z_1) and $\mathbf{x}_2$ (x_2, y_2, z_2) where the indices x, y, and z refer to the coordinates of a Cartesian coordinate system as indicated in Fig. 1. The detection of contacts between two particles is carried out in a straightforward fashion by checking the radii of two vicinity particles for overlap. Spheres 1 and 2 with radii R_1 and R_2 are taken to be in contact only if the distance D between their centers is less than the sum of their radii:

$$D \leqslant R_1 + R_2 \tag{1}$$

and

$$D = \sqrt{(x_1 - x_2)^2 + (y_1 - y_2)^2 + (z_1 - z_2)^2}. \tag{2}$$

The unit vector $\mathbf{e} = (\cos\alpha, \cos\beta, \cos\gamma)$ (see Fig. 1) is introduced as pointing from the center of sphere 1 to the center of sphere 2:

$$\mathbf{e} = \frac{\mathbf{x}_2 - \mathbf{x}_1}{D} = (\cos\alpha, \cos\beta, \cos\gamma), \tag{3}$$

where α, β, γ are the direction angles. Under zero loads, the particles will be in contact at a single point. As the load is increased, the particles deform in the vicinity of the point of initial contact such that the contact area will be finite but small compared to the particle size. The contact area is circular with a parabolic surface contact pressure distribution proposed by Hertz [5]:

$$p = p_0\sqrt{1 - \left(\frac{r}{a}\right)^2}, \tag{4}$$

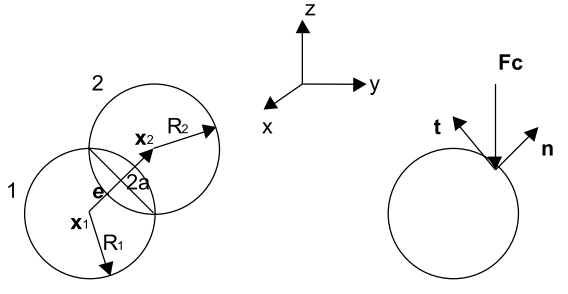

Fig. 1. Normal contact between two particles.

where a is the radius of the contact area and p_0 the contact pressure at $r = 0$. The resultant normal contact force F_n and contact pressure p_0 are given by Hertz theory [5] as

$$F_n = \frac{4E^*\sqrt{R\delta^3}}{3} \tag{5}$$

and

$$p_0 = \frac{3F_n}{2\pi a^2}, \tag{6}$$

where

$$\delta = R_1 + R_2 - D, \quad \delta = \frac{a^2}{R},$$
$$\frac{1}{E^*} = \frac{1 - v_1^2}{E_1} + \frac{1 - v_2^2}{E_2}, \tag{7}$$
$$\frac{1}{R} = \frac{1}{R_1} + \frac{1}{R_2},$$

R is the relative curvature, E_1 and E_2 are Young's moduli, v_1 and v_2 are Poisson's ratios, and R_1 and R_2 are the radii of the particles in contact, respectively. Hertz theory was first published in 1880s and has stood the test of time. A thorough experimental check on the validity of the Hertz theory showed that there was good agreement with the theoretical predictions of both contact force and internal stress up to the value of $a/R = 0.3$. This reassuring conclusion is rather surprising since this value of (a/R) corresponds to strains in the contact region rising to about 10% (on page 99 of [5]).

2.2. Shear stiffness k_s

The solution for shear force is more complicated, as it depends on the history of sliding and deformation at the contact. However, observations made during the tests described below suggest that it is unnecessary to represent the complete contact behavior in shear. The contribution of shear forces to the average deviatoric stress tensor is rather small in the tests, even for the highest friction used: the shear partition is found to account for less than 15% of the total deviatoric stress. The major contribution to deviatoric stress comes from the unequal distribution of normal forces around the particles. Furthermore, 30–40% of contacts are sliding, for most of the tests. Thus the effect of shear contact stiffness on bed behavior is likely to be small. In the following numerical model, the shear force, ΔF_s, is proportional to shear displacement, Δu_s, at each contact; the shear stiffness depends on normal force, and is equal to the initial loading stiffness, as given in [6,7]

$$\Delta F_s = k_s \Delta u_s \tag{8}$$

and

$$k_s = \frac{2G^{2/3}[6(1-v)RF_n]^{1/3}}{2-v}, \tag{9}$$

where G is the elastic shear modulus and v the Poisson ratio of the particles, respectively, which are given by

$$\frac{1}{G} = \frac{2-v_1}{G_1} + \frac{2-v_2}{G_2}, \qquad \frac{1}{v} = \frac{1}{2v_1} + \frac{1}{2v_2}. \tag{10}$$

2.3. Interface friction force

The friction at an interface has been traditionally described using Coulomb's friction law, which states that at incipient sliding, the friction force is given by

$$F_s = F_n \tan \phi_\mu, \tag{11}$$

where ϕ_μ is the interface friction angle. The values of the friction angle vary not only for material type, but also for test conditions and test apparatus. Although microscopic processes associated with interface friction have been explored, the interface friction phenomenon has not been completely understood [8]. In light of this, Coulomb's friction law and friction angle have served an important role in practice and are used in this modeling.

2.4. Particle motion law

The force–displacement law of a single particle will be developed for the simple 2D case first and then it will be extended to more complicated 3D situation. The normal contact force is calculated first; based on this information, the influence of the shear force or friction force is considered next. If only the normal contact force is considered, the x, y, and z components of the contact force, F_c, acting at contact point c, denoted as F_{xc}, F_{yc}, and F_{zc}, are related to F_c as

$$\mathbf{F}_c = \begin{pmatrix} F_{xc} \\ F_{yc} \\ F_{zc} \end{pmatrix} = \begin{pmatrix} F_n \cos\alpha \\ F_n \cos\beta \\ F_n \cos\gamma \end{pmatrix}. \tag{12}$$

Under quasi-static conditions, the inertial forces may be neglected and the equation of motion reduces to the following equilibrium condition:

$$\mathbf{F} - \sum_c \mathbf{F}_c = 0, \tag{13}$$

where $\boldsymbol{F}$ is the externally imposed force and the summation is performed over all contacts of the particle. Each particle in the assembly should satisfy the above equilibrium equation.

Considering the equilibrium of a particle, the interaction between the particle and surrounding particles in x-direction is simplified as a spring as indicated in Fig. 2.

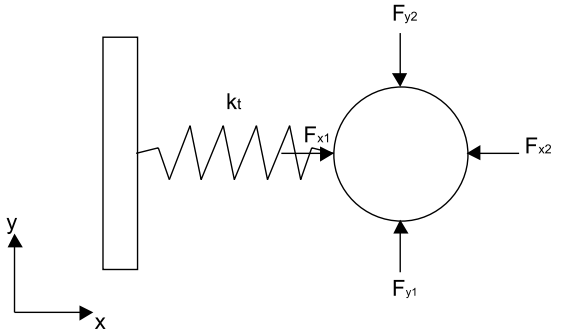

Fig. 2. Force equilibrium for a single particle.

Here the wall represents the external environment and the spring represents the interaction. Without considering the spring first, the net force in the x-direction is

$$F_x = F_{x1} - F_{x2}, \tag{14}$$

where F_{x1} and F_{x2} are the total positive and negative normal contact forces in the x-direction. If the normal contact forces at all contact points of the particle have been calculated through Hertz's theory (see Section 2.1), then

$$F_{x1} - F_{x2} = \sum_c F_{xc}, \tag{15}$$

where $\sum_c$ represents the summation over all contact points of the particle.

Similarly the total absolute force in the y-direction, which determines the shear stiffness and friction force, is given by

$$F_s = F_{y1} + F_{y2} = \sum_c |F_{yc}|. \tag{16}$$

The total stiffness in the x-direction is $k_n + k_s$ (normal stiffness k_n will be derived in Section 2.5), and the incremental displacement of the particle in the x-direction is given by Hooke's law as

$$\Delta D_x = \frac{F_x}{k_t} = \frac{\sum_c F_{xc}}{k_n + k_s}$$

for

$$\frac{k_s}{k_n + k_s}\left|\sum_c F_{xc}\right| < k_f \sum_c |F_{yc}| \tag{17}$$

otherwise

$$\Delta D_x = \frac{F_x - k_f|F_y|}{k_n} = \frac{\sum_c F_{xc} \pm k_f \sum_c |F_{yc}|}{k_n},$$

where $k_f = \tan\phi_\mu$ is the friction coefficient. The factor k_s is determined by (9), and varies from particle to particle or even from direction to direction for one particle due to the different shear force. Since the friction force is always at a direction that is opposite to the particle motion direction, the $\pm$ sign in the Eq. (17) should be

chosen such that the friction force is opposite to the active force ($\sum_c F_{xc}$).

Similarly, the incremental displacement in the y-direction is

$$\Delta D_y = \frac{F_y}{k_t} = \frac{\sum_c F_{yc}}{k_n + k_s}$$

for

$$\frac{k_s}{k_n + k_s}\left|\sum_c F_{yc}\right| < k_f \sum_c |F_{xc}| \tag{18}$$

otherwise

$$\Delta D_y = \frac{F_y - k_f|F_x|}{k_n} = \frac{\sum_c F_{yc} \pm k_f \sum_c |F_{xc}|}{k_n}.$$

For 3D, similar to the 2D situation, the incremental displacement of the particle in the x, y, or z-direction can be derived as

$$\Delta D_x = \frac{F_x}{k_t} = \frac{\sum_c F_{xc}}{k_n + k_s}$$

for

$$\frac{k_s}{k_n + k_s}\left|\sum_c F_{xc}\right| < k_f \sqrt{\left(\sum_c |F_{yc}|\right)^2 + \left(\sum_c |F_{zc}|\right)^2} \tag{19}$$

otherwise

$$\Delta D_x = \frac{F_x - k_f|F_t|}{k_n} = \frac{\sum_c F_{xc} \pm k_f \sqrt{\left(\sum_c |F_{yc}|\right)^2 + \left(\sum_c |F_{zc}|\right)^2}}{k_n},$$

$$\Delta D_y = \frac{F_y}{k_t} = \frac{\sum_c F_{yc}}{k_n + k_s}$$

for

$$\frac{k_s}{k_n + k_s}\left|\sum_c F_{yc}\right| < k_f \sqrt{\left(\sum_c |F_{zc}|\right)^2 + \left(\sum_c |F_{xc}|\right)^2} \tag{20}$$

otherwise

$$\Delta D_y = \frac{F_y - k_f|F_t|}{k_n} = \frac{\sum_c F_{yc} \pm k_f \sqrt{\left(\sum_c |F_{zc}|\right)^2 + \left(\sum_c |F_{xc}|\right)^2}}{k_n},$$

$$\Delta D_z = \frac{F_z}{k_t} = \frac{\sum_c F_{zc}}{k_n + k_s}$$

for

$$\frac{k_s}{k_n + k_s}\left|\sum_c F_{zc}\right| < k_f \sqrt{\left(\sum_c |F_{xc}|\right)^2 + \left(\sum_c |F_{yc}|\right)^2} \tag{21}$$

otherwise

$$\Delta D_z = \frac{F_z - k_f|F_t|}{k_n} = \frac{\sum_c F_{zc} \pm k_f \sqrt{\left(\sum_c |F_{xc}|\right)^2 + \left(\sum_c |F_{yc}|\right)^2}}{k_n}.$$

As in Eqs. (17) and (18), the $\pm$ signs in Eqs. (19)–(21) should be chosen such that the friction forces are opposite to the active force.

The displacement of each particle under external or internal loads is calculated based on Eqs. (19)–(21). Since any displacement of the neighboring contact particles would generate a new non-equilibrium situation, an iterative calculation of successive releasing of forces exerted on a single particle is performed until the resultant force on each particle in the assembly is sufficiently small.

2.5. Relaxation spring stiffness k_n

In Eqs. (19)–(21), the normal stiffness k_n of the relaxation spring still needs to be determined. It is related to the normal contact force between two particles in Eq. (5). To simplify the problem, a linear relationship is used to approximate the non-linear relationship of Eq. (5):

$$F = k_n \delta. \tag{22}$$

To better approximate Eq. (5) by Eq. (22), the least-square regression method is used. The square difference between Eqs. (5) and (22) is

$$\Delta = \int_0^{\delta_f} \left(\frac{4E^*\sqrt{R\delta^3}}{3} - k_n\delta\right)^2 d\delta. \tag{23}$$

To find the value of k_n such that Δ is the smallest, let $\partial\Delta/\partial k_n = 0$, then

$$k_n = \frac{8E^*\sqrt{R\delta_f}}{7}, \tag{24}$$

where δ_f is the average value of all δ_c at particle contact points.

2.6. Particle size distribution

To approximate the real particle size distribution, the particle size is varied by using two random numbers from a random number generator. If the particle radius is RR initially, the final particle radius is given by

$$R = RR * (1 + pr * \mathrm{RAND1} - pr * \mathrm{RAND2}), \tag{25}$$

where the RAND1 and RAND2 are two distinct random numbers each ranging from 0.0 to 1.0, pr ($0 \leqslant pr \leqslant 1.0$) is a parameter to control the range of particle size. If $pr = 0$, the assembly only has uniform sized particles of radius RR and if $pr = 1.0$, the particle radius ranges from 0.0 to 2.0 RR. Fig. 3 shows the particle size distribution of an assembly with 10 000 particles with $pr = 0.03$ and $RR = 0.5$ mm. The resultant particle size distribution is close to a Gaussian distribution.

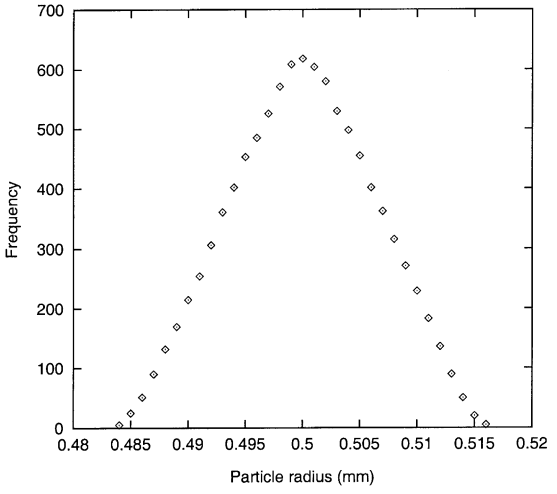

Fig. 3. Distribution of particle size for 10 000 particles.

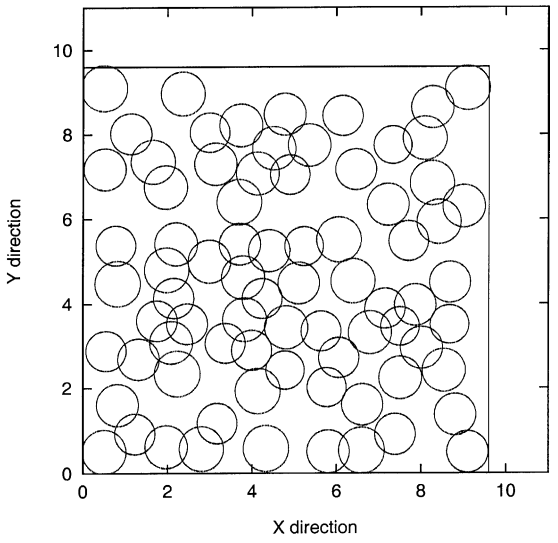

Fig. 4. Random interpenetrating particles with substantial overlaps and large free spaces.

2.7. Initial geometry generation

The program automatically generates the initial particle assembly. As input data, the total particle number, thermal properties, and mechanical behavior of solid particle material are given, as well as the parameter to control the particle size range. The dimensions of the assembly and the minimal and maximal particle radii are automatically calculated during the assembly generation process. The program can generate particle beds with two different structures: random packing and high-density face-centered regular packing. The procedures are described in the following paragraphs.

2.7.1. Isotropic random packed bed

To generate an isotropic random packed bed, first the computer program generates N random interpenetrating sphere particles in a cubic container, which has approximately N_x, N_y, and N_z units along x, y, and z-directions $(N_x * N_y * N_z = N)$, respectively. The distance between any two particles i and j is at least $0.7(R_i + R_j)$ to guarantee that no two particles are too close initially. This produces dispersion with a nominal solid fraction of 0.63, which has many overlaps; the majority of them are substantial (Fig. 4). To eliminate these overlaps, particles are moved according to Eqs. (19)–(21) with zero friction coefficients and zero shear stiffness to facilitate the particle movements. After approximately 20 000 iterations (requiring ~3 min on a 64-bit Digital Unix Workstation for 1000 particles), most of the substantial overlaps are eliminated. However, calculations show that there are large stresses (~9 MPa) exerted on container walls due to the initial high packing density of 63%. Next, the program slowly expands the cubic container to release the stresses exerted on it, as well as reduce the particle overlaps, until the final stress is less than 3.0×10^{-4} MPa. The final bulk density is approximately 60–62% depending on the particle size (large or small) and the deviation of the particle sizes. Fig. 5 shows the packed state for a particle assembly using a range of particle sizes between 0.5497 and 0.4452 mm. This state is taken as the initial equilibrium state for following loading and/or temperature rises.

2.7.2. An-isotropic face-center packed bed

The program can also generate a particle assembly of face-centered regular packing. Initially, the particle locations are given exactly according to the face-centered regular packing – which is also an equilibrium state for assembly with uniform particle sizes. Different from the isotropic random packed bed generated in previous section, the face-centered regular packed bed is an-isotropic, which means it exhibits different characteristics along different directions. The face-centered regular packing bed is only used for comparison purposes, since in reality particle beds never pack this way except when artificially arranged.

3. Thermomechanics characteristics of pebble beds – numerical results

The particle assembly is assumed to be bounded by six rigid walls that form a cubic volume. The loading is controlled by strain – the boundary elements move according to the corresponding strain. In the tests, the boundary elements are moved symmetrically with respect to the central axes of the particle assembly. The

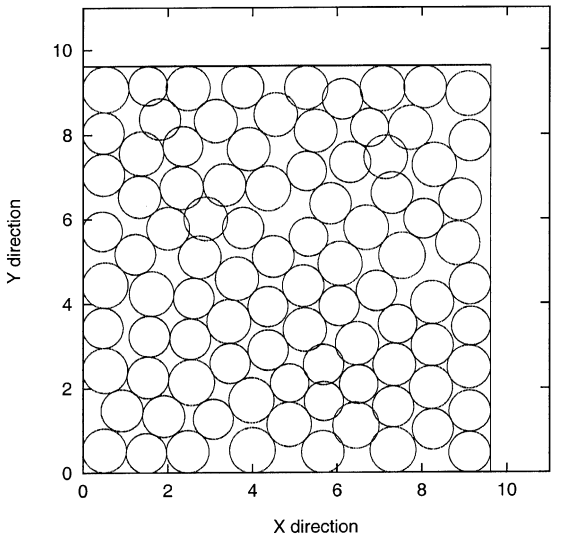

Fig. 5. Packing state after expanding the cubic container slowly to release the stress exerted on the container wall.

final particle position, contact forces, and macro-stresses are calculated after the equilibrium of the assembly is reached. Depending on the procedure, the next load and corresponding stresses may be taken and calculated. In all the simulations, Young's modulus, Poisson's ratio, and friction coefficients are obtained from handbook for typical beryllium or ceramic particle materials.

Fig. 6 shows the initial and final packed states under a uniaxial compressive strain of 3% for a packed assembly with initial packing shown in Fig. 5. Different particles move in different directions if initially the bed is randomly packed and particle sizes have some range. The corresponding strain field is not uniform even if the external loading is uniform (uniaxial compression). This is particularly noticeable for particles located next to the boundary. These results point out that the deformation of the particle material comes from the rearrangement of particles as well as the local deformation at contact points. Consequently, a portion of the deformation (rearrangement of particles) is plastic and is irreversible if the external loads are removed [9]. Fig. 7 shows the 3D space locations for the initial and final packed states under a hydrostatic compression of 3%. White represents the initial locations whereas red represents the final locations after 3% compression.

Fig. 8 shows the initial and final packed states under a 3% uniaxial compressive strain for a face-centered regular packed assembly using a uniform particle radius of 0.5 mm. For a regular-packed dense assembly of uniform size particles (initial density = 74%), the particles move only in the loading direction under uniaxial compression – the strain field in the particle assembly is almost uniform. The whole packed bed deforms like a continuum homogeneous material. This is due to the fact that, for a face-centered regular packing of 74% initial density, basically there is no free space for a given particle to move or enter. Consequently, the deformation of the packed bed mainly comes from the local deformation at the particle contact points rather than from particle relocation for random packed bed with

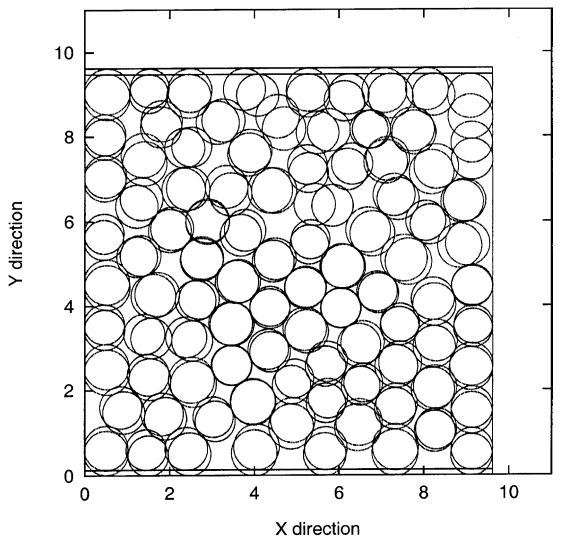

Fig. 6. Initial and final packed states under a uniaxial compressive strain of 3% (initial packing is shown in Fig. 5).

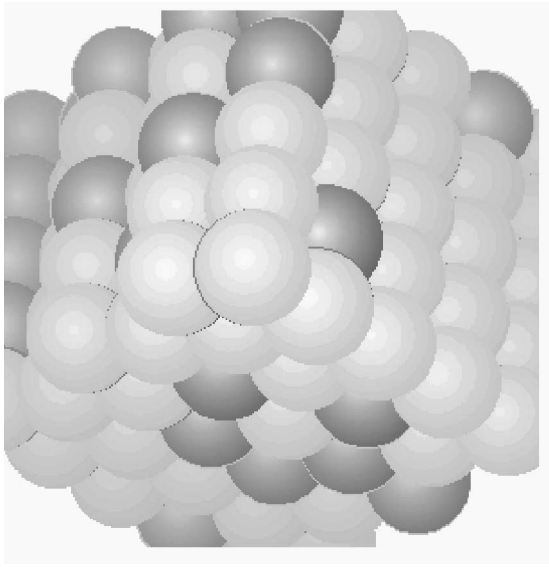

Fig. 7. 3D space locations for initial and final particle assembly (white represents the initial locations whereas the red represents the final locations after 3% compression).

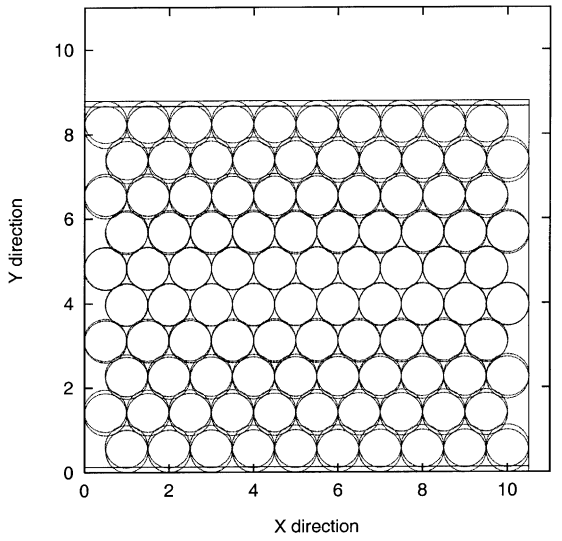

Fig. 8. Initial and final packed states under a uniaxial compressive strain of 3% for a particle assembly using uniform particle size (face centered regular packing, initial density = 74%).

lower initial density (61–63%). The result is a much stiffer packed bed.

The average wall stress as a function of compressive strain is illustrated in Figs. 9 and 10 for uniaxial compressions. It is a beryllium packed bed with average particle radius 0.5 mm, initial packing = 60%, and friction coefficient = 0.022 (Fig. 9), 0.2 (Fig. 10), respectively. For a packed bed with small friction coefficient under uniaxial compression, the corresponding stresses in the x, y, and z-directions are almost the same (Fig. 9). This is because, under a small friction coefficient, it is easy for particles to slide and enter the empty space in the assembly. Consequently, the packed bed behaves like a fluid and displays the same stresses in different directions. The variations in the curve gradient of Fig. 9 are due to local collapse of the fabric in particle assembly. It seems that local changes in fabric are significant even in a small number assembly. A portion of the deformation of the particle bed is a consequence of the displacement of particles and is irreversible, which indicates the change of state, and makes it imperative to define the mechanical behavior on the basis of state quantities.

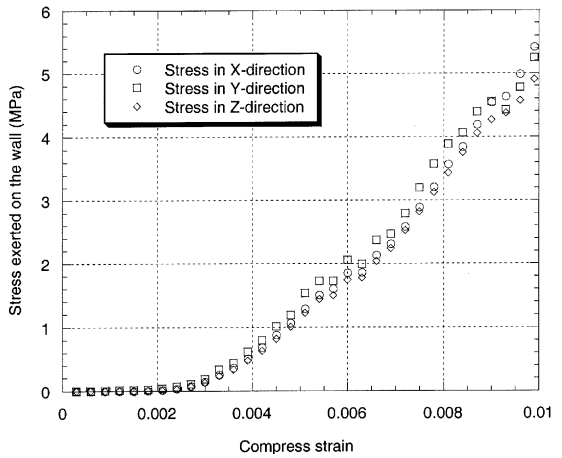

Fig. 9. Stress–strain relationship for uniaxial compression, beryllium packed bed, average radius = 0.5 mm, initial packing = 60%, Young's modulus = 249 GPa; Poisson's ratio = 0.07, friction coefficient = 0.022.

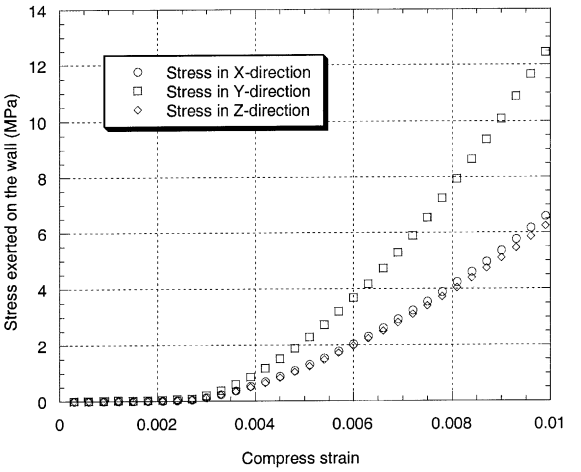

Fig. 10. Stress–strain relationship for uniaxial compression, beryllium packed bed, average radius = 0.5 mm, initial packing = 60%, Young's modulus = 249 GPa; Poisson's ratio = 0.07, friction coefficient = 0.2.

Conversely, for a packed bed with a large friction coefficient under uniaxial compression, the compressive stress (in the y-direction) is quite different from the lateral stresses in the x and z-directions (Fig. 10). This is because, under a large friction coefficient, the large friction force tends to prevent the sliding and motion of particles. Also the friction force between the particles and structural wall hinders the particle motion. The packed bed behaves more like a solid material and displays different stresses in compression and lateral directions. Despite the difference between compressive and lateral stresses, the discrepancy between the two lateral stresses σ_x and σ_z is small (Fig. 10). It proves that the initial packing is isotropic – even though the loaded packed bed displays an-isotropy between the y and x/z-directions, the behaviors in the x and z-directions are almost same, due to equal load (both have zero strains) applied in these directions.

3.1. Thermal stress due to particle bed temperature rise

The model as developed can be used to evaluate the maximum stress levels to which the bed particles and the wall are subjected due to bed thermal expansion. The particle overlap at the contact point due to thermal expansion is now calculated as

$$\delta = R_i(1 + \alpha\Delta T_i) + R_j(1 + \alpha\Delta T_j) - D_{ij}, \tag{26}$$

where D_{ij} is the distance between particle i and particle j along the normal direction, α is the thermal expansion coefficient of solid particle material, R_i and R_j are particle radii, and ΔT the bed temperature rise.

The container wall is assumed to be rigid without deformation under external force, which represents the worst-case scenario. The initial geometry is the same as that of Fig. 5. A beryllium packed bed is used with average particle radius 0.5 mm, initial packing = 60%, Young's modulus = 249 GPa, and Poisson's ratio = 0.07. The resultant thermal stress due to the larger bed thermal expansion, calculated as the force divided by area, exerted on the walls along the x, y, and z-directions for different increases in bed temperature is shown in Fig. 11. According to Hertz theory, the maximum shear stress in a particle, which happens beneath the center of contact surface ($r = 0$) at a depth of 0.48a, has a value of $0.31p_0$. Using this formula, the maximum shear stress is about 120 MPa for particle contacting the wall at highest temperature of 600 °C and the corresponding a/R value is ~0.2. Thus the modeling is still valid for this temperature situation since the experimental check on the validity of Hertz theory shows that there is a good agreement for both contact force and internal stress up to the value of $a/R = 0.3$ (on page 99 of [5]). If temperature keeps increasing as well as the stresses in particles, normal contact force relationship used in the modeling Eq. (5) needs to be changed due to two reasons: first the Hertz theory is probably not valid anymore for a/R larger than 0.3; second there is creep at high temperature. This subject is out of the scope of the paper.

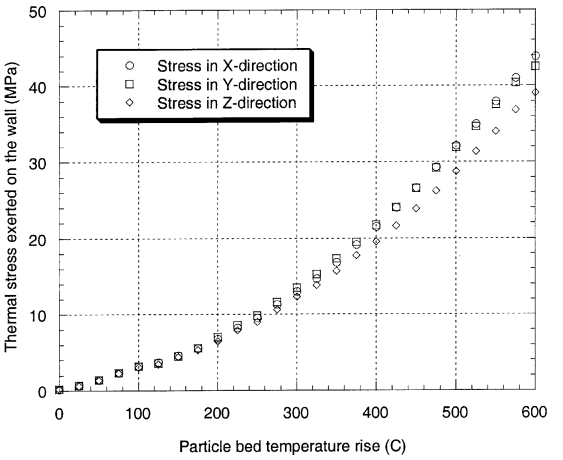

Fig. 11. Thermal stress exerted on the wall along x, y, and z-directions, beryllium packed bed, average radius = 0.5 mm, initial packing = 60%, Young's modulus = 249 GPa; Poisson's ratio = 0.07.

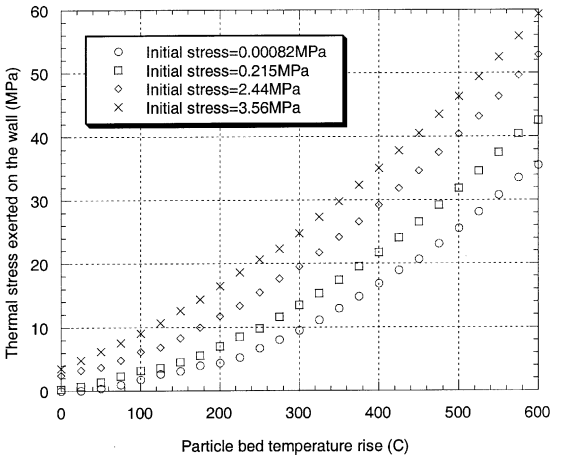

Fig. 12. Thermal stress exerted on the wall along the y-direction for different initial packing stress, beryllium packed bed, average radius = 0.5 mm, initial packing = 60%, Young's modulus = 249 GPa; Poisson's ratio = 0.07.

The stresses exerted on the wall for the various initial bed packing are shown in Fig. 12. It is seen that, as the initial packing stress increases (higher initial density), the thermal expansion stress increases greatly. This result implies that in selecting the initial bed density, compromise must be made – bed with higher initial density will have better heat transfer characteristics, which are beneficial, but higher thermal expansion stresses, which are detrimental to the reactor operations.

3.2. Verification of numerical simulations

The numerical calculations of the bed deformation modulus are compared with experimental results to check the validity of the modeling. The macroscopic incremental deformation modulus for uniaxial compression can be calculated as

$$E = \frac{\Delta\sigma}{\Delta\varepsilon}. \tag{27}$$

Figs. 13–15 show the calculated effective deformation modulus vs. the compression stress for Li_4SiO_4, Li_2ZrO_3, and beryllium pebble beds, respectively. Also given in those figures are Reimann's uniaxial compression [10] and the UCLA thermal expansion [11] experimental data for comparison. Reimann's experiment set-up, denoted

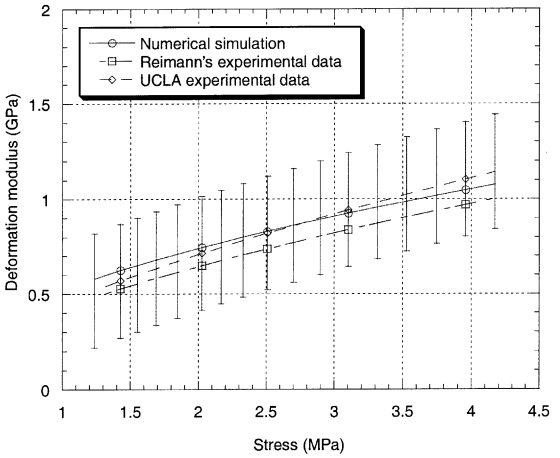

Fig. 13. Comparison of numerical calculated deformation modulus with experimental data obtained at UCLA and by Reimann et al. (Li_4SiO_4 packed bed, Young's modulus = 100.4 GPa, Poisson's ratio = 0.24, average radius = 0.22 mm, initial packing = 59%, friction coefficient = 0.3).

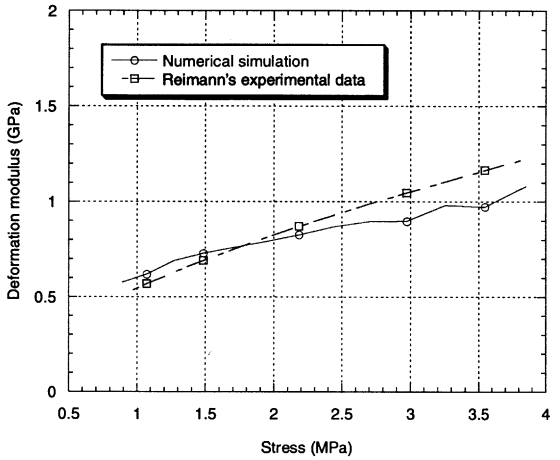

Fig. 14. Comparison of numerical calculated deformation modulus with experimental data obtained by Reimann et al. (Li_2ZrO_3 packed bed, Young's modulus = 117.6 GPa, Poisson's ratio = 0.2, average radius = 0.6 mm, initial packing = 59%, friction coefficient = 0.3).

SCATOLA, utilizes a cylindrical container and two plates to hold pebble beds of Li_4SiO_4, Li_2ZrO_3, and beryllium materials. A rod is connected to the lower plate and is allowed to slide within a tube that is connected to the upper plate. The relative movement of the two plates can be measured to derive the bed compaction, elastic–plastic properties. Whereas in UCLA's thermal expansion experiments, pebble beds are put into a cylindrical container. A load cell is used to measure the axial thermal expansion force when pebble beds are heated up (to 600 °C). Thermomechanical properties of bed materials

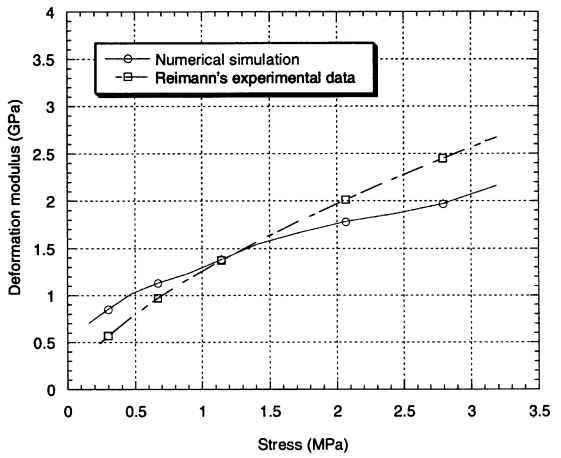

Fig. 15. Comparison of numerical calculated deformation modulus with experimental data obtained by Reimann et al. (Beryllium packed bed, Young's modulus = 276.9 GPa, Poisson's ratio = 0.07, average radius = 1.0 mm, initial packing = 59%, friction coefficient = 0.3).

can be derived based on the thermal expansion and calibration tests. Good agreements have been achieved between the numerical predictions and test data for both Reimann's and UCLA experiments. In general, the deformation modulus of packed bed material is 2–3 orders of magnitude smaller than that of solid material, in addition to being packing dependent.

4. Conclusion

A 3D numerical model has been developed to simulate the thermal and mechanical characteristics of packed beds in response to various loads and different particle parameters. The particle bed is modeled as a collection of rigid particles interacting via Hertz–Mindlin type contact. The model tackles the incremental movements of the constrained particles, which are caused by environmental changes such as temperature increases or external loads. Isotropically random packed beds were taken as the initial geometry for the following loading and/or temperature rises.

Macroscopically, the packed bed displays almost the same behavior in x, y, and z-directions for isotropic initial packing. By microscopically, different particles move in different directions even though the external loading is uniform (uniaxial or hydrostatic compression). The corresponding strain field in the particle assembly is not uniform. The deformation of the particle materials comes from the rearrangement of particles as well as the local deformation at contact points. The rearrangement of particles is irreversible even if the external loads are removed.

For particle material with a small friction coefficient, it is easy for particles to slide and enter the empty space in the assembly. Consequently, the packed bed behaves like a fluid and exerts same stresses on structural walls in different directions under uniaxial compression. Conversely, for particle material with a large friction coefficient, the large friction force tends to prevent the sliding and motion of particles. Also the large friction force between the particles and structural wall hinders the particle motion. The packed bed is stiffer and behaves more like a solid material.

Generally the macroscopic stress–strain relationships of packed beds are non-linear. The deformation modulus of packed bed material is 2–3 orders of magnitude smaller than that of solid material, in addition to being packing dependent. The calculated deformation modulus compares reasonably well with experimental data.

References

[1] P.A. Cundall, O.D.L. Strack, Geotechnique 29 (1) (1979) 47.
[2] P.A. Cundall, in: M. Satake, J.T. Jenkins (Eds.), Micromechanics of Granular Materials, Proceedings of US/Japan Seminar, October 26–30, 1987, Elsevier, Amsterdam, 1988, p. 113.
[3] Y. Kishino, in: M. Satake, J.T. Jenkins (Eds.), Micromechanics of Granular Materials, Elsevier, Amsterdam, 1988, p. 143.
[4] P.A. Serrano, J.M. Rodiriguez-Ortiz, in: Proceedings of Symp. Placticity and Soil Mechanics, Cambridge, 1973, p. 215.
[5] K.L. Johnson, Contact Mechanics, Cambridge University, London, 1985.
[6] R.D. Mindlin, Journal of Applied Mechanics 16 (1949) 259.
[7] R.D. Mindlin, H. Deresiewicz, J. Appl. Mech. 20 (1953) 327.
[8] I.L. Singer, H.M. Pollock, Fundamental of Friction: Macroscopic and Microscopic Processes, Kluwer Academic, Dordrecht, 1992.
[9] Feda, Jaroslav, Mechanics of Particulate Materials – The Principles, Elsevier, New York, 1982.
[10] J. Reimann, E. Arbogast, M. Behnke, S. Muller, K. Thomauske, in: 8th International Workshop on Ceramic Breeder Blanket Interactions, Colorado Springs, CO, USA, October 6–8, 1999.
[11] Z. Lu, A. Ying, M.A. Abdou, in: 8th International Workshop on Ceramic Breeder Blanket Interactions, Colorado Springs, CO, USA, October 6–8, 1999.